

Development and theoretical evaluation of an STF–SF isolator for seismic protection of structures

Minghai Wei · Gang Hu · Lixiao Li · Haitao Liu

Received: 28 March 2017 / Accepted: 26 October 2017 / Published online: 31 October 2017
© Springer Science+Business Media B.V. 2017

Abstract This study deals with the mechanical behavior of a shear thickening fluid–sliding friction (STF–SF) isolator, and investigates the feasibility of its application in anti-seismic engineering from a theoretical perspective. The STF–SF isolator is composed of a conventional sliding friction (SF) material and a smart shear thickening fluid (STF) material. When the excitation energy is small, the SF material keeps the structure static or only has a small vibration. However, when the excitation energy is large, the STF material results a huge damping force and dissipation of the external energy, eventually reducing the relative motion between the base and the upper structure. To better understand this phenomenon, a mechanistic

study of the STF–SF isolator is proceeded by an analytical model which is derived from flow momentum equations. After that, the seismic protective effect of the STF–SF isolator is evaluated at harmonic excitation with different accelerations through a single degree of freedom (SDOF) structure. Furthermore, the effects of layer gap, layer number and friction coefficient of the STF–SF isolator on the seismic protective effect are investigated. The results show that the STF–SF isolator can significantly decrease both the displacement response and the acceleration response of the SDOF structure. This theoretical study indicates the STF–SF isolator can be used in anti-seismic engineering.

M. Wei
Department of Construction and Engineering
Management, Shenyang Jianzhu University,
Shenyang 110168, China

G. Hu (✉)
Department of Civil and Environmental Engineering, The
Hong Kong University of Science and Technology,
Clear Water Bay, Hong Kong, China
e-mail: ghuaaust@gmail.com

L. Li
Guangdong Provincial Key Laboratory of Durability for
Marine Civil Engineering, Shenzhen University,
Shenzhen 518060, China

H. Liu
Shenzhen Graduate School, Harbin Institute of
Technology, Shenzhen 518055, China

Keywords Shear thickening fluid · Sliding friction · Smart · Isolator · Seismic protection

1 Introduction

If the input frequency of a seismic excitation matches the natural frequency of a structure, the structure will have a resonant reaction. This reaction can enlarge the relative displacement and acceleration of the upper parts of the structure, eventually causing structural damage. An effective and reliable technology to reduce structure responses caused by seismic excitations is base isolation [1]. However, traditional isolation bearings, such as laminated rubber and

sliding friction isolator bearing, cannot effectively reduce relative displacement, and may even enlarge it in some cases [2–6], such as near-fault earthquakes [2, 6] and far-field earthquakes [3]. To overcome the weakness, a number of studies attempted to adjust the stiffness and damping of the bearings by using smart materials to improve their isolation performance [7–10]. Smart materials that have been tested include electro-rheological (ER) fluids [7, 11], magneto-rheological (MR) fluid/elastomer [8, 9, 12–17] and shape memory alloy (SMA) [10, 18–21]. A common characteristic of these smart materials is that changing the material characteristics requires an external energy input. To ensure that these smart materials can provide large enough external energy, the isolation bearing that uses them may be large in volume, heavy, expensive, and structurally complicated.

A novel smart material named shear thickening fluid (STF) has been studied for the purpose of energy dissipation [22–29]. The STF is one type of highly concentrated colloidal suspension that consists of monodisperse particles suspended in a carrying fluid, and has the potential to exhibit both fluid and rigid behaviors when subjected to a sudden stimulus. That is to say the STF's mechanical properties (e.g. shear modulus, damping factor, etc.) change with stimuli. Moreover, as reported by Jiang et al. [30], the energy absorption and deformation processes of an STF are reversible. Because of these benefits, STFs have great potential for impact resistance and intelligent control in some engineering fields.

Lee et al. [22, 31] suggested that Kevlar[®] mats impregnated with STF show remarkably enhanced ballistic penetration resistance by adding the STF to the fabric. Park et al. [26] found that friction is the dominant energy absorption mechanism for fabrics impregnated with the STF during high-velocity impact. In addition, the energy absorption characteristics of STF-impregnated Kevlar[®] fabric specimens were studied using LS-DYNA [32]. For adaptive structure, Fischer et al. [29, 33] investigated the tuning part stiffness and damping capacity of a sandwich beam with STFs core under free vibration by experimental and finite element analysis (FEA) methods. The forced vibration of a sandwich beam integrating an STF core and with conductive skins subjected to a periodic excitation was investigated by Wei et al. [27]. The results show that the natural frequency of the sandwich beam integrating the STF is dynamic rather

than invariant under different periodic excitations, which is very different from conventional structures. To study the vibration suppression capabilities of STFs, Pinto and Meo [24] developed an engineered STF, which can be embedded directly as an active layer within the fibrous reinforcement of a composite laminate, to manufacture stiff carbon fiber reinforced plastic (CFRP) parts characterized by higher levels of energy absorption. Iyer et al. [28] proposed a micro-scale actuator immersed in STFs and found that the vibration velocity of the actuator can be saturated when actuation forces are large enough. Based on the unique features of STFs, Zhang et al. [34] designed a prototype STF damper in the flow mode to study its dynamics. They found that the dynamic loading velocity has a significant influence on the energy absorption response and stiffness. Zhou et al. [35] experimentally investigated the dynamic characteristics of an STF damper with different STF mass fractions and revealed that the dissipated energy per cycle of STF damper is much higher than the other dampers, which implies a better performance of the STF damper for shock absorption or impact resistance. Aimed at the earthquake resistance, the performance of an STF-filled damper was tested under different ground acceleration conditions by Yeh et al. [36], and was observed that both area and shape of the hysteresis loop in the STF-filled damper vary with loading conditions. However, to the authors' best knowledge, STFs are still rarely applied in civil engineering. This is because at a long range of lower shear rate, the viscosity value of STFs is very small (seen in Fig. 1), which may reduce the civil engineering safety under environmental excitations.

Based on the constant friction characteristic of sliding friction (SF) materials and considered as compensation material for the STFs, this study design a new, smart high-energy dissipation composite isolator called "shear thickening fluid–sliding friction (STF–SF) isolator". The mechanical properties and characteristics of the STF–SF isolator are investigated by an analytical model, and the seismic performance of a single degree of freedom (SDOF) system with the STF–SF isolator under harmonic excitations with different ground accelerations are further evaluated. Its aim is to illustrate the feasibility of STF–SF isolator in anti-seismic engineering applications from a conceptual approach.

The study is organized as follows: in Sect. 2, one-dimensional constitutive experiment parameters

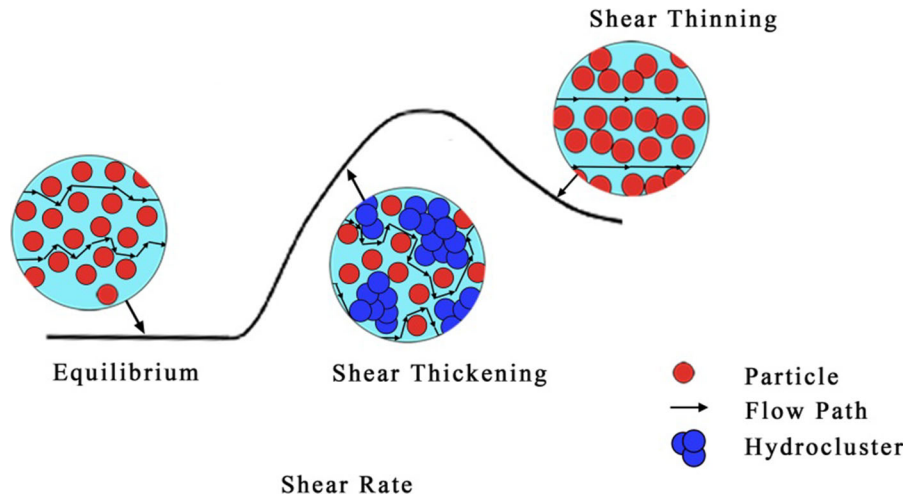


Fig. 1 Schematics of shear thickening fluid

proposed by Zhang et al. [34] is employed to formulate the complex viscosity of the STF; in Sect. 3, after introducing the design of an STF–SF isolator, an analytical model of the STF–SF isolator using a parallel plate model is presented, and the mechanical performances of the STF–SF isolator are investigated; in Sect. 4, an SDOF system is taken as an example, and the seismic protective effects of the STF–SF isolator are discussed under harmonic excitations with different accelerations. Then, some key parameters of the STF–SF isolator for the seismic protective effect are investigated. Finally, concluding remarks are given in Sect. 5.

2 Shear thickening fluid

The rheology properties of STF used in the present study are obtained from Zhang et al. [34]. In their experiments, the STF solvent is prepared by using fumed silica nanoparticles and ethylene glycol. The fumed silica (S5505, from Sigma-Aldrich) has a primary particle size of 14 nm and a surface area of approximately 200 m²g⁻¹, and the ethylene glycol has a density of 1.113 g ml⁻¹ (102,466, ReagentPlus[®], from Sigma-Aldrich). The rheology properties of STF with different mass fractions under 25 °C is measured by a parallel-plate rheometer (MCR 301, Anton Paar Companies, Germany). The diameter of the parallel plate is 20 mm, and the thickness is set to 0.2 mm.

More details of the experimental setup can be found in Zhang et al. [34].

To predict the viscosity curve of STFs, which changes continuously with the increasing shear rate, and further show the integrity of the mechanical performance of the STF–SF isolator, a phenomenological model that possesses equivalent viscosity characteristics is proposed.

$$\eta(\dot{\gamma}) = \eta_0 + \frac{\eta_{\max} \left(1 - \frac{1}{1 + \exp(a\dot{\gamma} + b)} \right)}{1 + \exp(c\dot{\gamma} + d)} \quad (1)$$

where a , b , c , d , η_0 and η_{\max} are the parameters obtained from the experiments with STF materials, and $\dot{\gamma}$ denotes the shear rate.

The parameters for the continuous model in Eq. (1) are chosen to be $\eta_0 = 0.16793$, $\eta_{\max} = 28.51281$, $a = -0.00073$, $b = 2.327$, $c = -0.01817$, and $d = 7.0885$, which fit the viscosity curve of the proposed model to the STF with 30% mass fractions in the Ref. [34]. The predicted curve is then compared with the corresponding experimental data, as shown in Fig. 2. Apparently, the proposed STF model predicts the viscosity behavior accurately in all regions. Its characteristics include both the shear thickening behavior at high shear rates and the shear thinning behavior at high enough shear rates.

For a power-law fluid, the relationship of the shear rate and velocity in the parallel plate mode can be written as

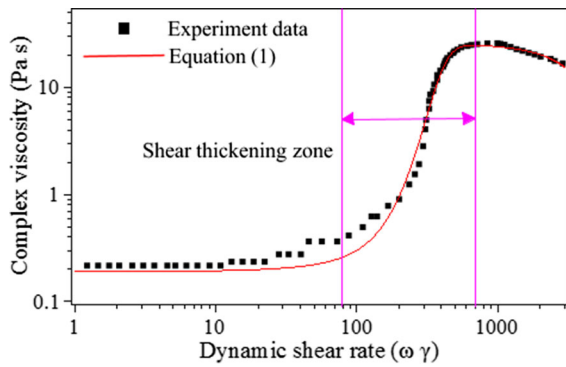


Fig. 2 Apparent modulus function of the complex viscosity of the STF compared to experiment data from Ref. [34] at 30 wt% and 25 °C

$$\dot{\gamma} = \frac{V(t)}{\Delta h} \tag{2}$$

where $V(t)$ is the velocity of plate and Δh is the gap between the parallel plates.

3 STF–SF isolator

3.1 Design of STF–SF isolator

The design process and characteristics of the STF–SF isolator are described in this section. Here, the main purpose is to evaluate the protection effectiveness of the STF–SF isolator under seismic excitation, rather than discussing the sensitive behavior of the materials to environment, e.g. temperature. Thus, some possible accessory equipment, such as thermostatic device, is not considered in the sketch design. The sketch of the isolator is shown in Fig. 3. As can be seen in Fig. 3a, b, the STF–SF isolator is composed of an upper member, lower member, sealing coil, STF and SF materials. The upper member is formed by connecting an upper connecting plate and a column part (formed by laminated steel plate shown in Fig. 3c), and the lower member is formed by the end face of the hollowed cylinder and the lower connecting plate. The upper member is mutually matched with the hollowed column of the lower member through the SF layer, so that the column part is in the interior of the hollowed column, which is filled with STF. On the other hand, referring to Fig. 3d, the column part at the two ends of the isolator limits the sliding displacement of the isolation layer.

3.2 Simplified mathematical model

Figure 3c shows the laminated steel plate column part in the STF–SF isolator. As shown in Fig. 3c, the part is formed by connecting multiple layers of steel plates through a cylinder, and each space between the steel plates is filled with the STF. The length, width and height of each plate are l , b and H , respectively. The gap between the plates is denoted by h . The whole laminated steel plate column member has N steel plates, and thus, the number of the gaps between the plates is $(N + 1)$. Because the diameter of the cylinder is smaller than the width of the steel plate, the influence of the column is negligible when the analytical model of the STF–SF isolator is established. Meanwhile, the following assumptions were made: (1) the fluid flow is continuous, incompressible and fully developed; (2) the fluid properties are homogeneous within the interval l of the fluid action section, hence it can be considered as a one-dimensional problem; (3) the fluid is in the state of a laminar flow; (4) the ratio between the layer gap and its width is very small so that the fluid flow can be approximated by the flow between the parallel plates.

Based on the above assumptions, the stress and velocity profiles through a parallel plate model (between two steel plates) can be described in Fig. 4. Then, the governing equation of motion for the movement of the STF is obtained by using the flow momentum equations as follows:

$$\rho \left(\frac{\partial u}{\partial t} + u \frac{\partial u}{\partial x} + v \frac{\partial u}{\partial z} \right) = \frac{\partial \sigma_{xx}}{\partial x} + \frac{\partial \tau_{xz}}{\partial z} \tag{3}$$

where u and v are the flow velocities of the STF in the x and z directions, respectively; $\partial \sigma_{xx} / \partial x$ and $\partial \tau_{xz} / \partial z$ are the pressure gradients in the x and z directions, respectively; ρ is the density of the STF.

According to the parallel plate’s assumptions, the STF is a one-dimensional flow in the x direction, thus $v = 0$ and $\partial \sigma_{xx} / \partial x = -dp/dx$. On the other hand, the flow velocity in the x direction is invariant in terms of the flow continuity, namely $\partial u / \partial x = 0$. Furthermore, the inertia of the STF is ignored and thus $\partial u / \partial t = 0$. Consequently, Eq. (3) can be simplified to

$$\frac{\partial \tau_{xz}}{\partial z} = \frac{dp}{dx} \tag{4}$$

where dp/dx is the pressure gradient and $\partial \tau_{xz}$ denotes the shear stress in the z direction.

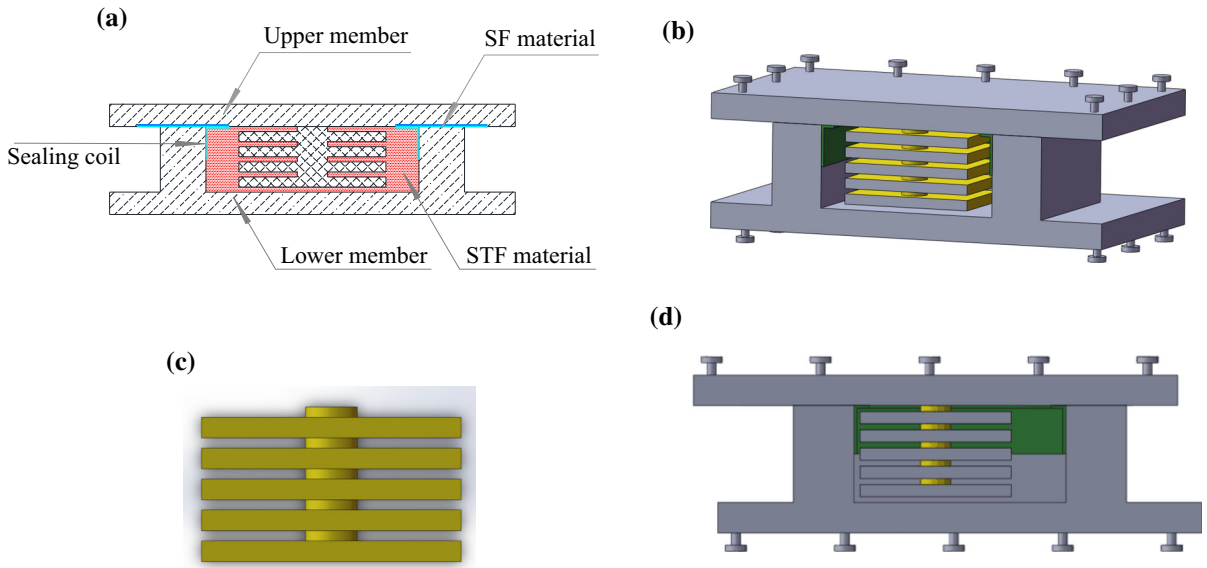


Fig. 3 Detailed sketch of an STF-SF isolator. **a** Sketch of STF-SF isolator. **b** Three-dimensional partial sectional view. **c** Laminated steel plate column part. **d** Deformation of the isolator

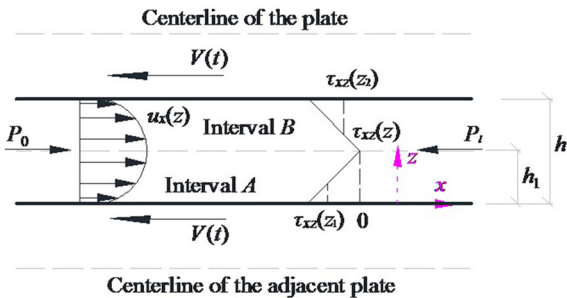


Fig. 4 Stress and velocity profiles through a parallel plate model

The solution can be written as

$$\tau_{xz}(z) = \frac{dp}{dx}z + C \tag{5}$$

in which C denotes a constant, and can be determined using boundary conditions.

In the interval A , the shear rate has the following expression

$$\dot{\gamma} = \frac{du_{x,A}}{dz} \tag{6}$$

Thus, the shear stress can be written as

$$\tau_{xz}(z) = \eta\dot{\gamma} = \eta \frac{du_{x,A}}{dz} \tag{7}$$

where η denotes the viscosity of the fluid.

Substituting Eqs. (7) into (3), integrating about z , and then considering the boundary conditions of $u_{x,A}(0) = -V(t)$ and $\tau_{xz}(h_1) = 0$, the flow velocity of the STF in the x direction can be obtained as

$$u_{x,A}(z) = \frac{1}{2\eta} \frac{dp}{dx} \left(h_1^2 - (h_1 - z)^2 \right) - V(t) \tag{8}$$

$(0 \leq z \leq h_1)$

where $V(t)$ denote the velocity of parallel plates.

In the interval B , similar to the manipulations for obtaining Eq. (8), and considering the boundary conditions of $u_{x,B}(h) = -V(t)$ and $\tau_{xz}(h_1) = 0$, the flow velocity of the STF in the x direction is given as

$$u_{x,B}(z) = \frac{1}{2\eta} \frac{dp}{dx} \left((h - h_1)^2 - (z - h_1)^2 \right) - V(t) \tag{9}$$

$(h_1 \leq z \leq h)$

The volume flow rate Q has the following form

$$Q = b \int_0^h u_x(z) dz = A_p V(t) \tag{10}$$

where A_p is the action area of the plate.

Substituting Eqs. (1), (2), (8) and (9) into (10), and considering $h_1 = h/2$, the relationship between the plate velocity and the damping force can be obtained

$$F_{\text{STF-P}}(t) = \frac{12A_p l (A_p + bh)}{bh^3} \times \left(\eta_0 + \frac{\eta_{\max} \left(1 - \frac{1}{1 + \exp\left(\frac{V(t)a}{h} + b\right)} \right)}{1 + \exp\left(\frac{V(t)c}{h} + d\right)} \right) V(t) \quad (11)$$

where $F_{\text{STF-P}}(t)$ denotes the damping force of the STF between the parallel plates.

For the sake of computation and analysis, the model of sliding friction force adopted the sequential friction model presented by Mostaghel and Davis [37].

$$F_{\text{SF}}(t) = \mu \tanh(\alpha V(t)) Mg \quad (12)$$

in which μ is the friction coefficient, M is the mass of the structure, g is the gravitational acceleration and α is a constant (usually, more than 100).

Thus, considering the physics parameters fitted from by Zhang et al. [34], the damping force model of the STF–SF isolator can be written as

$$F_{\text{STF-SF}}(t) = (N + 1) \frac{2.01516(A_p + \frac{1}{2}bh)A_p l V(t)}{bh^3 \left(1 + \exp\left(7.0885 - \frac{0.01817V(t)}{h}\right) \right)} \times \left(\left(1 + \exp\left(7.0885 - \frac{0.01817V(t)}{h}\right) \right) + 169.7899 \left(1 - \frac{1}{1 + \exp\left(2.327 - \frac{0.00073V(t)}{h}\right)} \right) \right) + \mu \tanh(\alpha V(t)) Mg \quad (13)$$

where N denotes the number of the plate layers.

3.3 Mechanical performance of the STF–SF isolator

The mechanical performance of the STF–SF isolator with various system parameters are investigated in this section. A superstructure with a total mass of $M = 103.78 \times 10^5$ kg and a total weight of $Mg = 101.71 \times 10^3$ kN [38] was taken as an example. Based on the Chinese Standards [39, 40], the physical parameters of the evaluated STF–SF isolator were set as follows: $l = 0.25$ m, $b = 0.25$ m, $H = 0.015$ m and $N = 10$. The gap between the plates was defined as $h = 1.0$ mm so that the STF can exhibit the shear thickening behavior. On the other hand, to keep the structure stationary under a smaller

seismic excitation, the friction coefficient was set to $\mu = 0.04$ and $\alpha = 2000$ according to the code for seismic design of buildings [41]. To elaborate the working principle of the isolator, the force–velocity performances of the SF, STF and STF–SF isolators were all investigated.

Since the force–velocity curve is anti-symmetric with respect to the origin, only the force–velocity curves at the positive-velocity range are shown in Fig. 5. As shown in Fig. 5a, the force–velocity curve of the STF, which overlaps with the STF–SF curve, exhibits a nonlinear behavior with increasing velocity. Beyond a critical velocity, approximately 0.3 m/s, the damping force of the STF increases remarkably. Moreover, the damping force generated by the STF is very large, e.g. 8.5×10^6 kN when the velocity is 3 m/s. However, the friction force of the SF is only about 705 kN, and it is much smaller than the damping force generated by the STF, and can even be ignored. The above phenomena show that the STF has a significant nonlinear energy dissipation capacity, and no external energy input is required. However, Fig. 5a also shows that the STF material has a weakness that the damping force of the STF is very small when the vibration velocity is small. This is because the shear thickening behavior does not occur in the STF, and the damping force is only derived from the normal flow of liquid. Figure 5b is a local magnification of Fig. 5a in the velocity range from 0 to 0.04 m/s. As can be seen, when the velocity is less than 0.02 m/s, the damping force of the STF is less than the friction force of the SF. With decreasing velocity, the damping force of the STF approaches to 0, whereas the friction force of the SF generally keeps constant, about 705 kN.

Based on the constant friction characteristic of the SF and the excellent energy dissipation capacity of the STF at large velocities, the STF–SF isolator is proposed. As shown in Fig. 5a, when the velocity exceeds a critical value, about 0.16 m/s, the force–velocity curve of the STF–SF isolator in general overlaps with that of the STF. Therefore, beyond the critical velocity, the influence of the friction force of SF on the STF–SF isolator is negligible, and the STF–SF isolator mainly exhibits the high energy-dissipation characteristic. Moreover, in Fig. 5b, when the velocity is small, the minimum damping force of the STF–SF isolator increases to the friction force generated by the SF at a relatively smaller velocity. This indicates that

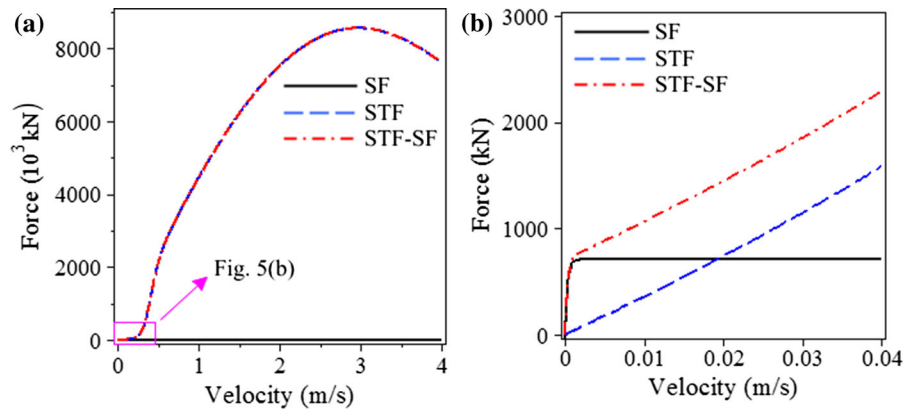


Fig. 5 Force–velocity performance of the STF–SF isolator. **a** Force–velocity response. **b** Local magnification of Fig. 5(a)

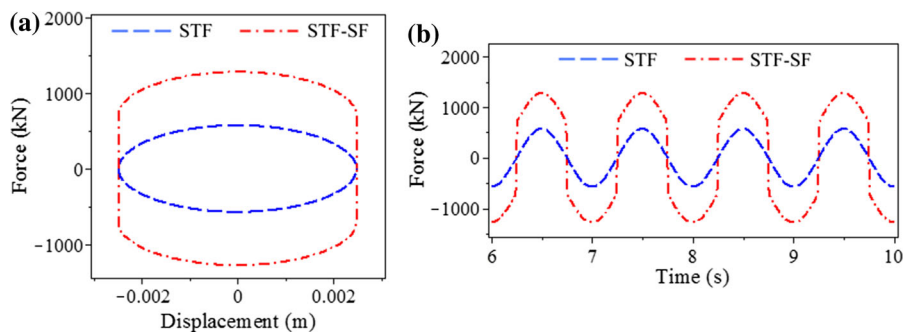


Fig. 6 Mechanical performance of the STF–SF isolator with 0.01 g acceleration and 1.0 Hz frequency. **a** Force–displacement response. **b** Force–time response

the energy-dissipation capacity of the STF–SF isolator has been enhanced at a relatively smaller velocity.

Figure 6a, b show the force–displacement and force–time responses of the STF and STF–SF isolators subjected to a harmonic excitation with an acceleration of 0.01 g and a frequency of 1.0 Hz. From Fig. 6a, the force–displacement response of the STF exhibits a similar ellipse feature, and the significant increases with increasing excitation. However, at the two ends of the isolator, due to the decrease of the excitation, the damping force of the STF becomes small, and even close to zero. For this scenario, using the STF isolator to control structure vibrations is very unfavorable. However, the force–displacement curve of the STF–SF isolator surrounds that of the STF, and the maximum damping force is 1277 kN, 223.6% of the STF force. Moreover, the minimum damping force of the STF–SF isolator at the end of the isolator is increased to the value of the damping force provided by the SF. Figure 6b shows the force–time curve of the

STF–SF isolator and compares it to the curve of the STF isolator. Due to the SF in the STF–SF isolator, the damping force of the STF–SF isolator always exists. Moreover, the force–time curve of the STF–SF isolator still shows the periodic feature under a harmonic excitation, which indicates that the addition of the SF does not affect the periodic properties of the STF–SF isolator.

When the acceleration increased to 1.4 g, the force–displacement and force–time responses of the STF and STF–SF isolators are shown in Fig. 7. As shown in Fig. 7a, b, the force–displacement and force–time curves of the STF and STF–SF isolators completely overlap with each other, which imply that the SF material results in a negligible effect on the STF–SF isolator when the excitation is very strong. Compared to Fig. 6a, the force–displacement curve of the STF–SF isolator becomes fuller and tends to be a rectangle, indicating that the STF–SF isolator has a larger energy-dissipation capacity.

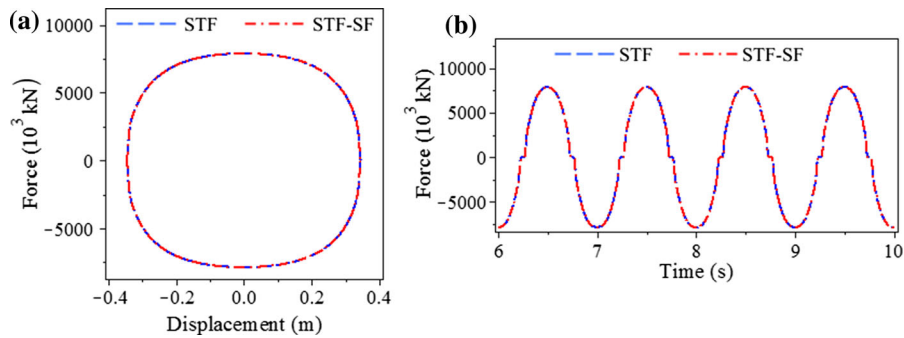


Fig. 7 Mechanical performance of the STF–SF isolator with 1.4 g acceleration and 1.0 Hz frequency. **a** Force–displacement response. **b** Force–time response

4 Seismic protection of structure

In this section, taking an SDOF structure as an example, the application feasibility of the STF–SF isolator in the anti-seismic engineering will be discussed. On one hand, since the seismic ground motion can be constituted by some harmonic loads, the seismic protective effect of the STF–SF isolator for an SDOF structure subjected a harmonic ground motion will be investigated.

4.1 Equations of the SDOF system

Considering an SDOF structure subjected to a seismic ground acceleration $\ddot{X}_g(t)$, the equation of motion with STF–SF isolator is given by

$$M\ddot{X}(t) + C\dot{X}(t) + KX(t) = -M\ddot{X}_g(t) - F_{STF-SF}(t) \tag{14}$$

where M , C , K and $X(t)$ are the mass, damping, stiffness and displacement of the SDOF structure, respectively; $\ddot{X}_g(t)$ is the ground acceleration; and $F_{STF-SF}(t)$ is the damping force of the STF–SF isolator.

For an earthquake, the expression of harmonic load in ground motion can be defined as

$$\ddot{X}_g(t) = W \sin(\omega t) \tag{15}$$

where W and ω is the ground motion amplitude and frequency, respectively.

Substituting Eqs. (13) into (14), and considering the mechanism of sliding friction, the equation of motion is expressed as

$$\begin{aligned} M\ddot{X}(t) = & -M\ddot{X}_g(t) - \frac{(N + 1)2.01516(A_p + bh)A_pIV(t)}{bh^3 \left(1 + \exp\left(7.0885 - \frac{0.01817V(t)}{h}\right)\right)} \\ & \times \left(\left(1 + \exp\left(7.0885 - \frac{0.01817V(t)}{h}\right)\right) \right) \\ & + \frac{28.51281}{0.16793} \left(1 - \frac{1}{1 + \exp\left(2.327 - \frac{0.00073V(t)}{h}\right)} \right) \\ & - \mu \tanh(\alpha V(t))Mg \end{aligned} \tag{16}$$

4.2 Effectiveness evaluation of the STF–SF isolator for the seismic protection

Figures 8, 9 and 10 show the dynamic behaviors of an SDOF system with an STF–SF isolator under a harmonic ground acceleration with various amplitudes but with one frequency of 1.0 Hz. The physical parameters and material properties of the evaluated STF–SF isolator are identical with those set in Sect. 3.3. From Fig. 8a, under the harmonic excitation with an acceleration of 0.01 g, the displacement curve of the STF–SF isolator nearly has no drift, but the curve of pure STF isolator shows a slight swing. This implies that the STF–SF isolators have a better protective ability. Further, referring to Fig. 8b, the displacement curve center of the STF–SF is close to 0.01 m, and its amplitude is only 0.001 m, which is 1/10 times that of the STF isolator.

Figure 8c shows the acceleration response of an SDOF system with STF or STF–SF isolators under a harmonic excitation. The protective effect of the STF isolator for the acceleration is relatively poor; the decrease ratio is only 40%. However, the STF–SF isolator has an almost perfect protective effect; the

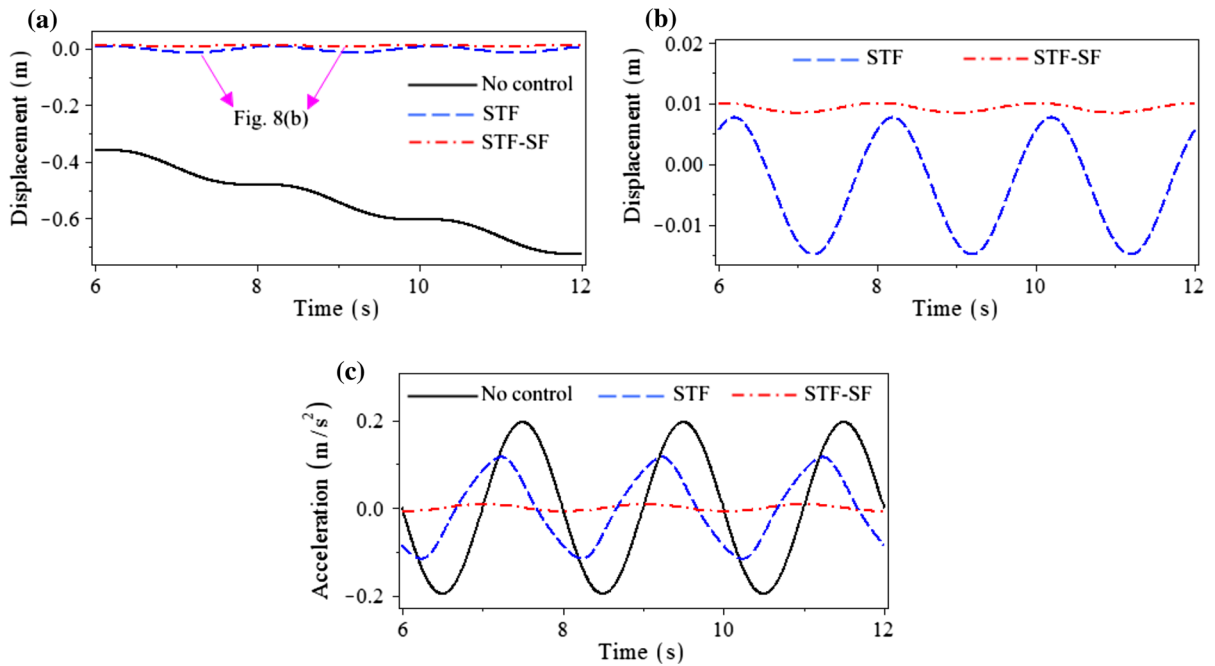


Fig. 8 Protection effectiveness of the STF–SF isolator under a harmonic excitation with 0.01 g acceleration. **a** Displacement response. **b** Local magnification of (a). **c** Acceleration response

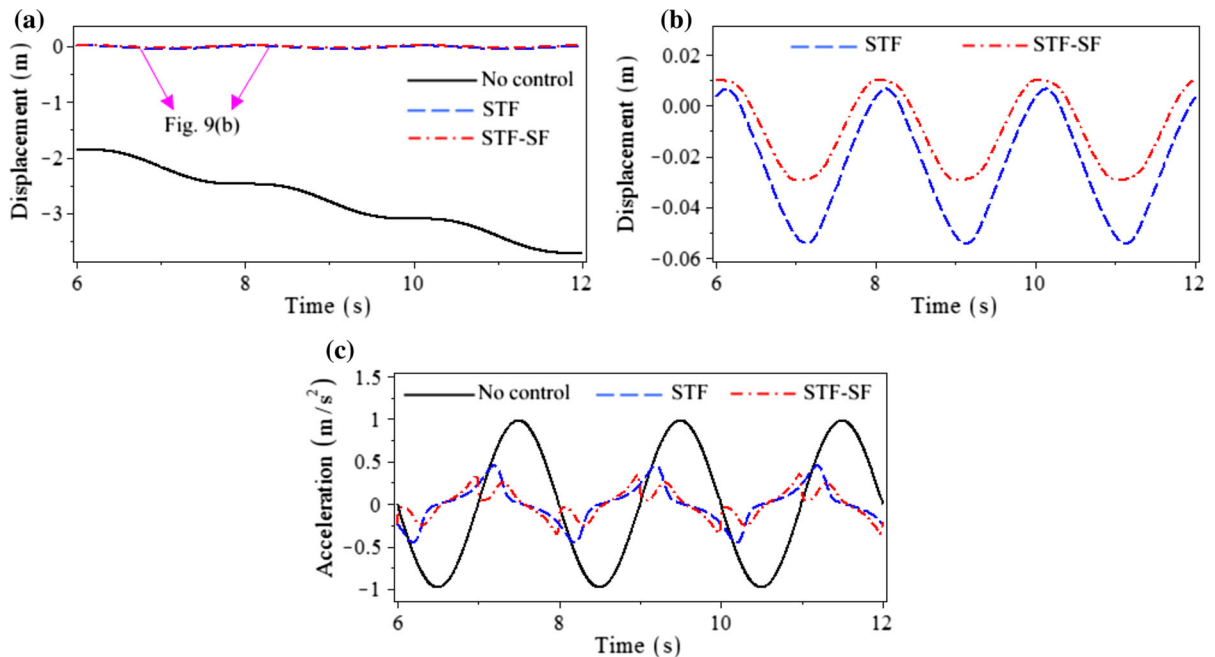


Fig. 9 Protection effectiveness of the STF–SF isolator under harmonic excitation with 1.0 g acceleration. **a** Displacement response. **b** Local magnification of (a). **c** Acceleration response

acceleration curve only has a slight fluctuation and the decrease ratio reaches 96%. Therefore, it can be

concluded that the STF–SF isolator can effectively protect the systems against a small seismic excitation

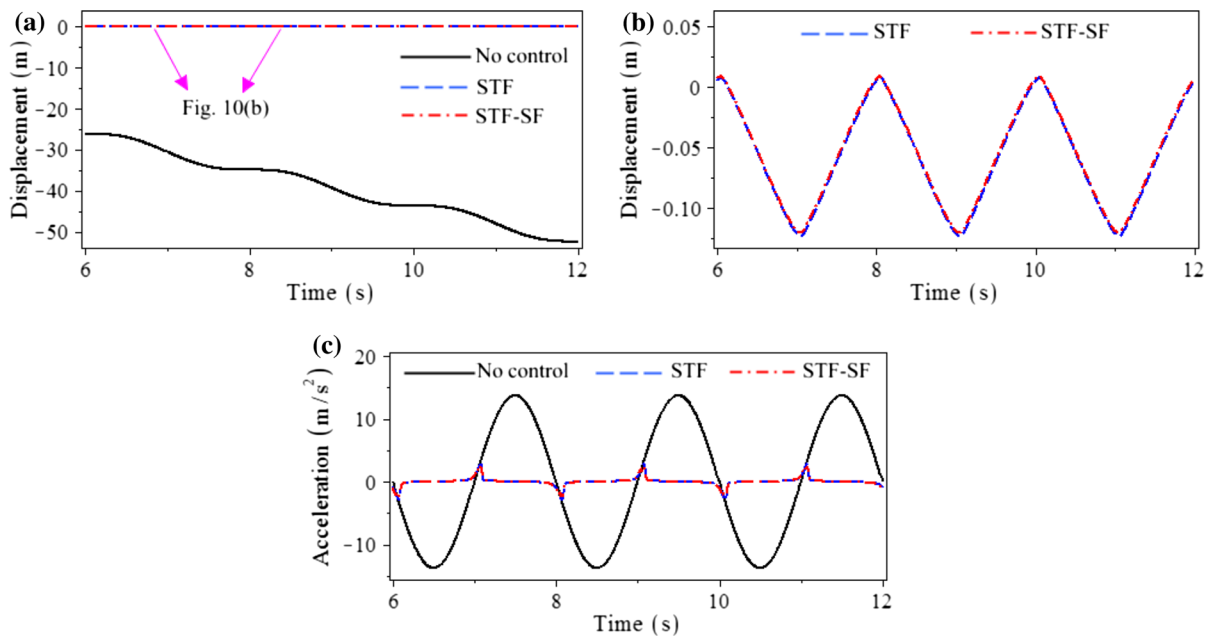


Fig. 10 Protection effectiveness of the STF–SF isolator under harmonic excitation with 1.4 g acceleration. **a** Displacement response. **b** Local magnification of (a). **c** Acceleration response

at two aspects of displacement and acceleration due to the existence of SF material supplies the energy dissipation capacity to the whole isolator.

When the ground acceleration is increased to 1.0 g, Fig. 9 shows the displacement and acceleration responses of an SDOF system with the STF or STF–SF isolators subjected to a harmonic excitation. From Fig. 9a, the displacement curves of the STF and STF–SF are both in the vicinity of 0 m and do not show much fluctuation, indicating that both the STF and STF–SF isolators have a better protective effect compared to Fig. 8a. This is because the viscosity of the STF has increased sharply due to its shear thickening behavior, which occurs under this much larger harmonic excitation. However, since the STF is just changed from solution to a state close to solid due to the shear thickening, the viscosity does not increase to the maximum value. Thus, the STF–SF isolator still exhibits superiority. As shown in Fig. 9b, the STF–SF isolator can further decrease the displacement of the SDOF system. The maximum displacements of the STF and STF–SF are 0.054 and 0.029 m, respectively.

For controlling the acceleration, referring to Fig. 9c, both the STF and STF–SF isolators can effectively decrease the acceleration response of the SDOF system. The acceleration decrease ratio of the

STF isolator is about 54.1%, and the ratio of the STF–SF isolator reaches 64.3% due to the contribution of the SF’s friction. Thus, the STF–SF isolator exhibits a better protective effect than the STF isolator.

In fact, when the ground acceleration continues to increase, the contribution of the SF material in the STF–SF isolator decreases and even disappears. Figure 10 shows the protective effect of the STF and STF–SF isolators under a harmonic excitation with 1.4 g acceleration. Both the STF and STF–SF isolators exhibit a significantly effective protection to the SDOF system when it is subjected to a larger seismic excitation. The displacement decrease ratios of both the STF and STF–SF isolators are close to 100%, and the acceleration decrease ratios reach 79.3 and 82.4% for the STF and STF–SF isolators, respectively. Referring to Fig. 10b, the displacement curves of the STF and STF–SF isolators overlap with each other except slight differences in the peak value, which indicates that the contribution of the SF material is very small. The reason of the above phenomenon is that the STF is changed from liquid state to solid state and a full development makes its viscosity larger.

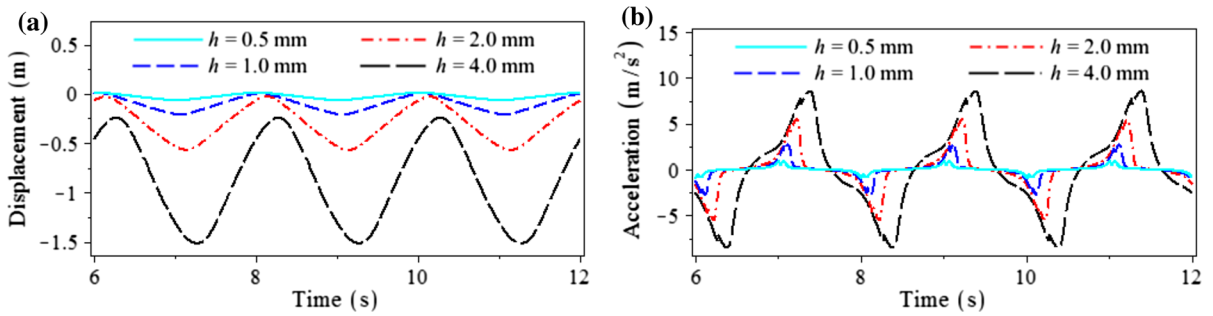


Fig. 11 Effect of layer gap on the protective effect of the STF–SF isolator with $N = 10$ and $\mu = 0.04$. **a** Displacement response. **b** Acceleration response

4.3 Some key parameters analysis

To extend the application range of the STF–SF isolator, the protective effects of the STF–SF isolator with different physical parameters are studied when the SDOF structure is subjected to a harmonic excitation with a 1.0 g ground acceleration and 1.0 Hz frequency. The physical parameters and material properties of the evaluated STF–SF isolator are identical with those set in Sect. 3.3 except the parameters of h , N and μ .

4.3.1 Effect of the layer gap

Figure 11 shows the effect of layer gap on the protective effect of the STF–SF isolator based on displacement and acceleration responses. It can be seen that the layer gap has a significant effect on the protective effect of the STF–SF isolator. When the layer gap $h = 4$ mm, both displacement and acceleration responses have large amplitudes, 1.51 m and 5.53 m/s². However, the two responses decrease with

decreasing the layer gap; the two responses decrease to 0.07 m and 0.89 m/s², only 4.6 and 16.1% of those for $h = 4$ mm respectively when the layer gap is reduced to 0.5 mm. Apparently, the layer gap is a very effective control parameter for the STF–SF isolator.

4.3.2 Effect of layer number

Figure 12 shows the effect of number of the layer on the protective effect of the STF–SF isolator. The displacement and acceleration responses of the SDOF structure decrease with increasing the layer number. Moreover, this decrease is nonlinear. For instance, for the acceleration response, when the number of the layer N is increased from 5 to 10, the acceleration is decreased by 81.8%. From 10 to 20 and from 20 to 40, it is decreased by 85.7 and 87.5% respectively. It is worth noting that when the layer number reaches 40, the SDOF structure has almost no response. Therefore, the layer number has a significant effect on the protective effect.

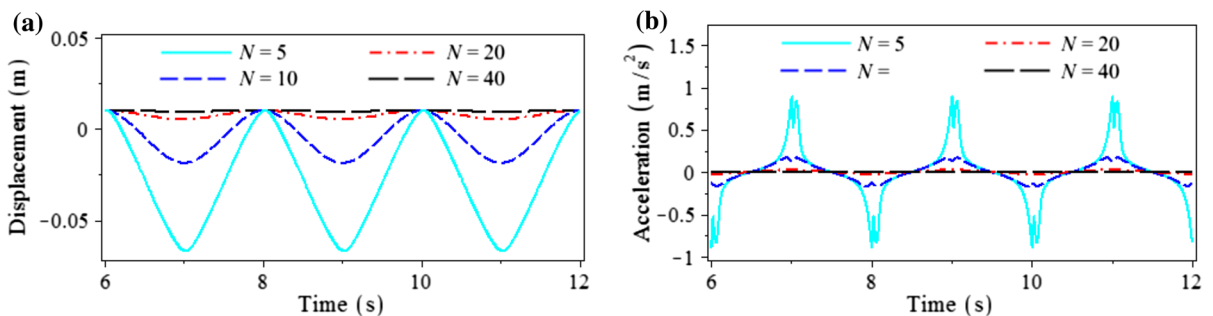


Fig. 12 Effect of layers on the protective effect of the STF–SF isolator with $h = 1.0$ mm and $\mu = 0.04$. **a** Displacement response. **b** Acceleration response

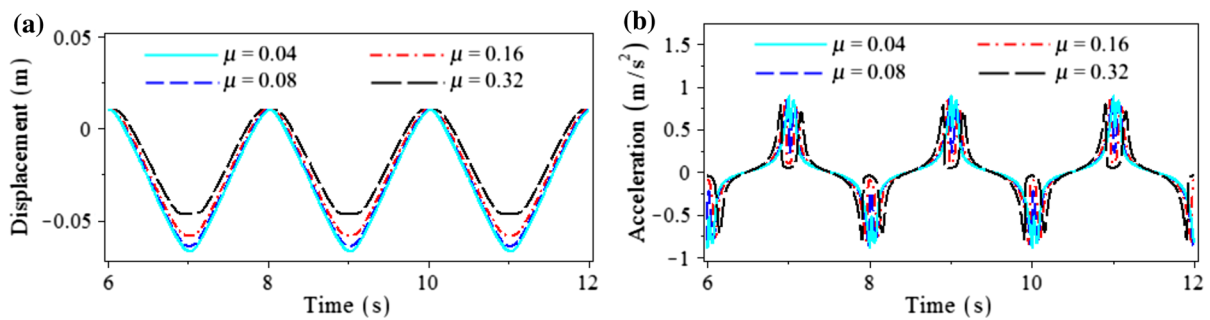


Fig. 13 Effect of friction coefficient on the protective effect of the STF-SF isolator with $h = 1.0$ mm and $N = 10$. **a** Displacement response. **b** Acceleration response

4.3.3 Effect of friction coefficient

The effect of friction coefficient on the protective effect of the STF-SF isolator is shown in Fig. 13. As can be seen in Fig. 13a, the friction coefficient only has effects on the displacement response. When the friction coefficient is increased from 0.16 to 0.32, the displacement is only decreased by about 19.0%. Compared to the effect of the layer gap and layer number, this value is very small. On the other hand, referring to Fig. 13b, the friction coefficient results in a slight effect on the acceleration response when the friction coefficient increases. It can be concluded that an increase in the friction coefficient cannot provide an effective control, especially for the acceleration response.

5 Conclusions

The study investigates the mechanical behavior of an STF-SF isolator, and aims to discuss the feasibility of its application in anti-seismic engineering from a theoretical perspective. Based on the flow momentum equations, an analytical model is firstly derived to investigate the force-displacement and force-velocity characteristics of the STF-SF isolator under different acceleration excitations. Then, the dynamic responses of an SDOF system with the STF-SF isolator subjected to harmonic excitations are investigated to determine the effectiveness of the isolator for the seismic protection. Finally, the effects of some key parameters on the seismic protective effect are evaluated.

Based on the investigation results, the following conclusions are made:

1. Although the damping force of a single STF isolator increases sharply when the excitation exceeds one threshold, the force is very small below this threshold. Therefore, the single STF isolator cannot be widely used in seismic protection engineering. By contrast, due to the existence of the SF material, the minimum damping force of the STF-SF isolator increases to the value of the friction force generated by the SF. Moreover, when the excitation is larger, the influence of SF's sliding friction characteristics on mechanical performance of the STF-SF isolator is negligible, and the STF-SF isolator still exhibits the high energy dissipation characteristic.
2. The STF-SF isolator is able to provide a very effective protective effect for the SDOF system regardless of the intensity acting seismic excitation. Especially when the structure is subjected to a very small or very large seismic excitation, the STF-SF isolator can exhibit an almost perfect protective behavior.
3. Both the layer gap and number of the STF-SF isolator have a significant effect on the seismic protective effect. However, the protective effect increases with decreasing the layer gap but with increasing the layer number. Compared to the effect of layer gap and layer number, the friction coefficient of the STF-SF isolator has only a less significant effect on the seismic protective effect. However, taking into account the sliding friction of SF is a supplement to the damping force of the single STF isolator when the structure subjected a smaller excitation. Therefore, the friction coefficient should be considered as smaller, as long as it can keep the structure from moving under a smaller seismic excitation.

In the next work, a finite element model based on the experiment data of the STF–SF isolator will be proposed. Coupled with the finite element model, a cable-stayed bridge with STF–SF isolator subjected near-fault seismic excitations will be investigated and discussed.

Acknowledgements The authors are extremely grateful to the anonymous reviewers for their valuable comments and suggestions for improving the quality of the present study as well as future work.

Funding This study was funded by the National Natural Science Foundation of China (Grant No. 51608335), China Postdoctoral Science Foundation (Grant No. 2016M591432), and Shenzhen Knowledge innovation program basic research Projects (Grant No. JCYJ20140417172417115).

Compliance with ethical standards

Conflict of interest The authors declare that they have no conflict of interest

Human and animals rights The research involving no human participants and/or animals

Appendix

In order to demonstrate the feasibility of the presented model for the STF–SF isolator, the method adopted in this study is used to establish another analytical model of a STF damper, and a comparison is made between the analytical model and the results of the Ref. [36].

A schematic of the STF damper is shown in Fig. 14. The effective fluid annular gap is the entire annular space between the piston’s outside diameter and the inside of the damper cylinder’s housing. Thus, the STF is pushed through the annular gap when the piston moves forward or backward. The overall length and the effective axial pole length of the damper are denoted by L and l , respectively. The outside diameter

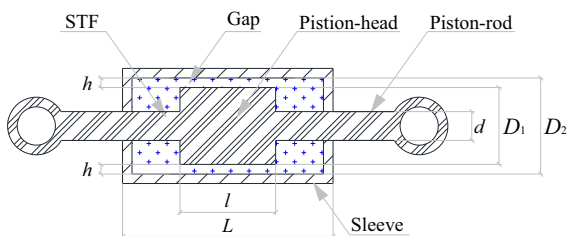


Fig. 14 Schematic of the STF damper

and inside diameter of the piston are denoted by D_1 and d , respectively. Considering the gap distance of h , the inside diameter of the damper cylinder’s housing can be written as $D_2 = D_1 + 2h$. For the theoretical analysis of STF dampers, some assumptions are made and consistent with the current study (Fig. 15).

Adopting the method of the current study, the relationship between the damping force and piston velocity can be obtained

$$F(V) = \frac{12\eta(\dot{\gamma})A_p l}{bh^3} \left(A_p + \frac{1}{2}bh \right) V(t) \tag{17}$$

in which $\eta(\dot{\gamma})$ denotes the viscosity of STF material.

Combining the experiment data from Yeh et al. [36], the apparent modulus function of the STF has the following form

$$\eta(\dot{\gamma}) = 0.3273 + \frac{21.9636 \left(1 - \frac{1}{1 + \exp(-0.0362\dot{\gamma} + 1.0821)} \right)}{1 + \exp(-0.2098\dot{\gamma} + 2.4385)} \tag{18}$$

where $\dot{\gamma}$ is the shear rate. Comparison between Eqs. (1) and (18) shows that the two equations have the same expression except the different parameters.

For a parallel plate model, the shear rate can be expressed as

$$\dot{\gamma} = \frac{V(t)}{h} \tag{19}$$

where $V(t)$ is the velocity of piston and h is the gap distance.

According to the Ref. [36], the excitation defines as follows

$$w(t) = W \sin(\omega t) \tag{20a}$$

$$V(t) = W\omega \cos(\omega t) \tag{20b}$$

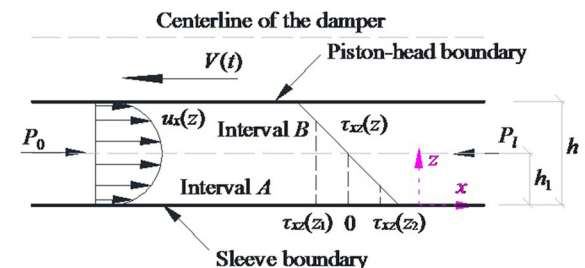


Fig. 15 Stress and velocity profiles through a parallel plate model

where W and ω are the excitation amplitude and frequency, respectively. Then, substituting Eqs. (18) to (20a, b) into (17), the damping force of the damper can be calculated.

From Fig. 16a, b, the theoretical complex viscosity based on Eq. (18) agree well with the experimental result. Moreover, Eq. (18) can well reflect the shear thickening behavior of the STF. However, when the shear rate is small, such as $\dot{\gamma} < 10 \text{ s}^{-1}$, the function does not agree well with the data. This phenomenon makes the results of the analytical model presented in the manuscript unreasonable. Therefore, the results of the analytical model when the shear rate is small are not discussed.

According to Ref. [36], the physical parameters of the STF damper are set as follows: $D_1 = 0.1 \text{ m}$, $D_2 = 0.098 \text{ m}$, $l = 0.1 \text{ m}$ and $h = 0.002 \text{ m}$. Since the

diameter of the piston-rod was not given in this reference, it is estimated to $d = 0.03 \text{ m}$.

Figure 17 shows comparison of the analytical model of the STF damper and experimental data of the Ref. [36]. From Fig. 17a, b, the force–displacement curve based on the analytical model agrees well with the experimental data, such as the approximate horizontal and stable characteristics, except the tilt behavior at the two ends of the damper and a slight difference in the specific damping force value. The tilt behavior may be caused by the installation of experiment since the STF is a fluid and no stiffness. For the slight difference in specific damping force value, this is because that the annular gap has a significant influence on the damping force value of the STF damper, which has concluded in this study (seen in Fig. 11). If the annular gap of the STF damper in the

Fig. 16 The apparent modulus function of the complex viscosity of the STF compared to the experiment data from the Ref. [36]. **a** Linear coordinate. **b** Double logarithm coordinates

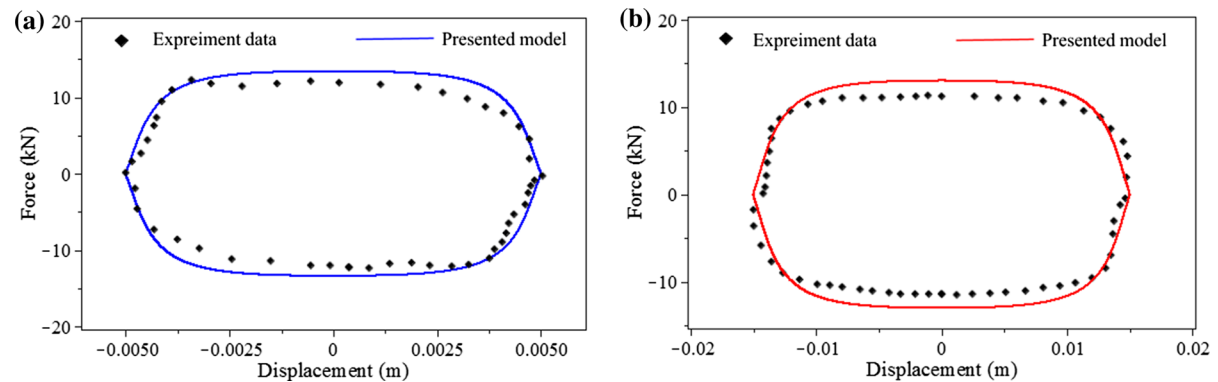
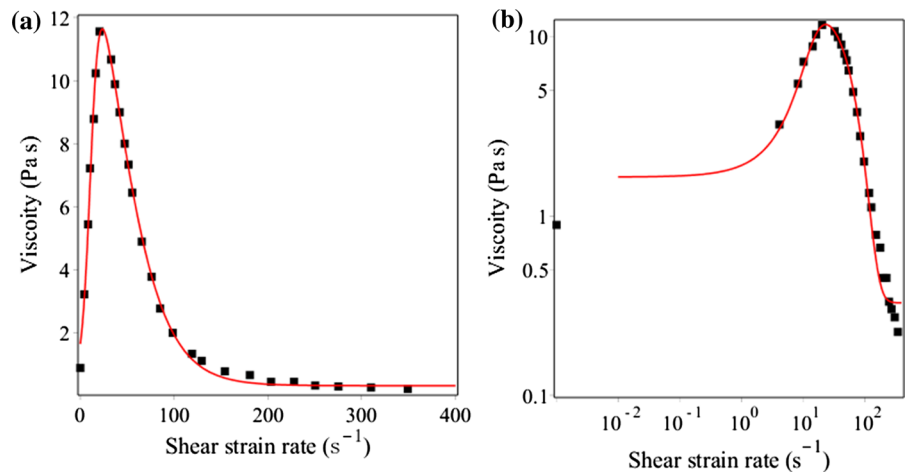


Fig. 17 Comparison of results between the analytical model and the Ref. [36]. **a** 5 mm stroke and 3.0 Hz frequency. **b** 15 mm stroke and 1.0 Hz frequency

experiment does not have enough machining precision or the materials of the STF damper is not smooth enough, the damping force value will be changed greatly.

Based on the above analysis, the analytical model of the STF damper is valid. Therefore, the presented model of the STF–SF isolator is also effective and feasible.

References

- Skinner RI, Robinson WH, McVerry GH (1993) An introduction to seismic isolation. Wiley, New York
- Kelly JM (1999) The role of damping in seismic isolation. *Earthq Eng Struct Dyn* 28:1717–1720
- Abdalla JA, Petrovski JT, Mohamedzein EA (2008) Vibration characteristics of a far field earthquake and its shaking effects on Dubai emerging skyscrapers. In: The 14th world conference on earthquake engineering, Beijing, China
- Satish N, Sriram N, Erik J (2008) Structural control benchmark problem: phase II-nonlinear smart base-isolated building subjected to near-fault earthquakes. *Struct Control Health Monit* 15:653–656
- Jangid RS, Kelly JM (2010) Base isolation for near-fault motion. *Earthq Eng Struct Dyn* 30:691–707
- Mazza F, Vulcano A (2012) Effects of near-fault ground motions on the nonlinear dynamic response of base-isolated r.c. framed buildings. *Earthq Eng Struct Dyn* 41:211–232
- Shih M-C, Wang T-Y (2008) Active control of electro-rheological fluid embedded pneumatic vibration isolator. *Integr Comput Aided Eng* 15:267–276
- Li Y, Li J, Tian T, Li W (2013) A highly adjustable magnetorheological elastomer base isolator for applications of real-time adaptive control. *Smart Mater Struct* 22:095020
- Yang J, Sun S, Tian T, Li W, Du H, Alici G, Nakano M (2016) Development of a novel multi-layer MRE isolator for suppression of building vibrations under seismic events. *Mech Syst Singal Process* 70–71:811–820
- Mekaouche A, Chapelle F, Balandraud X (2016) Using shape memory alloys to obtain variable compliance maps of a flexible structure: concept and modeling. *Meccanica* 51:1287–1299
- Oh H-U, Onoda J, Minesugi K (2004) Semiactive isolator with liquid-crystal type ER fluid for momentum-wheel vibration isolation. *J Vib Acoust* 126:272–277
- Stelzer GJ, Schulz MJ, Kim J, Allemang RJ (2003) A magnetorheological semi-active isolator to reduce noise and vibration transmissibility in automobiles. *J Intell Mater Syst Struct* 14:743–765
- York D, Wang X, Gordaninejad F (2007) A new MR fluid-elastomer vibration isolator. *J Intell Mater Syst Struct* 18:1221–1225
- Wang W, Song Y (2012) Nonlinear vibration semi-active control of automotive steering using magneto-rheological damper. *Meccanica* 47:2027–2039
- Yu Y, Li Y, Li J (2015) Parameter identification and sensitivity analysis of an improved LuGre friction model for magnetorheological elastomer base isolator. *Meccanica* 50:2691–2707
- Nurul AAW, Mazlan SA, Kamaruddin S, Nik INI, Choi SB, Amirul HRS (2016) Fabrication and investigation on field-dependent properties of natural rubber based magneto-rheological elastomer isolator. *Smart Mater Struct* 25:107002
- Yu Y, Li Y, Li J, Gu X (2016) A hysteresis model for dynamic behaviour of magnetorheological elastomer base isolator. *Smart Mater Struct* 25:055029
- Attanasi G, Auricchio F, Fenves GL (2009) Feasibility assessment of an innovative isolation bearing system with shape memory alloys. *J Earthq Eng* 13:18–39
- Jeong H-K, Han J-H, Youn S-H, Lee J (2014) Frequency tunable vibration and shock isolator using shape memory alloy wire actuator. *J Intell Mater Syst Struct* 25:908–919
- Mondal PD, Ghosh AD, Chakraborty S (2017) Control of underground blast induced building vibration by shape-memory-alloy rubber bearing (SMARB). *Struct Control Health Monit*. <https://doi.org/10.1002/stc.1983>
- Gur S, Mishra SK, Chakraborty S (2014) Performance assessment of buildings isolated by shape-memory-alloy rubber bearing: comparison with elastomeric bearing under near-fault earthquakes. *Struct Control Health Monit* 21:449–465
- Lee BW, Kim CG (2012) Computational analysis of shear thickening fluid impregnated fabrics subjected to ballistic impacts. *Adv Compos Mater* 21:177–192
- Waitukaitis SR, Jaeger HM (2012) Impact-activated solidification of dense suspensions via dynamic jamming fronts. *Nature* 487:205–209
- Pinto F, Meo M (2016) Design and manufacturing of a novel shear thickening fluid composite (STFC) with enhanced out-of-plane properties and damage suppression. *Appl Compos Mater* 24:1–18
- Majumdar A, Butola BS, Srivastava A, Bhattacharjee D, Biswas I, Laha A, Arora S, Ghosh A (2016) Improving the impact resistance of p-aramid fabrics by sequential impregnation with shear thickening fluid. *Fiber Polym* 17:199–204
- Park JL, Yoon BI, Paik JG, Kang TJ (2012) Ballistic performance of p-aramid fabrics impregnated with shear thickening fluid; Part II—effect of fabric count and shot location. *Text Res J* 82:542–557
- Wei M, Hu G, Jin L, Lin K, Zou D (2016) Forced vibration of a shear thickening fluid sandwich beam. *Smart Mater Struct* 25:055041
- Iyer SS, Vedad-Ghavami R, Lee H, Liger M, Kavehpor HP, Candler RN (2013) Nonlinear damping for vibration isolation of microsystems using shear thickening fluid. *Appl Phys Lett* 102:251902
- Fischer C, Braun SA, Bourban PE, Michaud V, Plummer CJG, Manson JAE (2006) Dynamic properties of sandwich structures with integrated shear-thickening fluids. *Smart Mater Struct* 15:1467–1475
- Jiang WF, Gong XL, Xuan SH, Jiang WQ, Ye F, Li XF, Liu TX (2013) Stress pulse attenuation in shear thickening fluid. *Appl Phys Lett* 102:101901
- Lee YS, Wetzel ED, Wagner NJ (2003) The ballistic impact characteristics of Kevlar (R) woven fabrics impregnated

- with a colloidal shear thickening fluid. *J Mater Sci* 38:2825–2833
32. Park Y, Kim Y, Baluch AH, Kim C-G (2015) Numerical simulation and empirical comparison of the high velocity impact of STF impregnated Kevlar fabric using friction effects. *Compos Struct* 125:520–529
 33. Fischer C, Bennani A, Michaud V, Jacquelin E, Manson JAE (2010) Structural damping of model sandwich structures using tailored shear thickening fluid compositions. *Smart Mater Struct* 19:035017
 34. Zhang XZ, Li WH, Gong XL (2008) The rheology of shear thickening fluid (STF) and the dynamic performance of an STF-filled damper. *Smart Mater Struct* 17:035027
 35. Zhou H, Yan LX, Jiang WQ, Xuan SH, Gong XL (2014) Shear thickening fluid-based energy-free damper: design and dynamic characteristics. *J Intell Mater Syst Struct* 27:1–13
 36. Yeh FY, Chang KC, Chen TW, Yu CH (2014) The dynamic performance of a shear thickening fluid viscous damper. *J Chin Inst Eng* 37:983–994
 37. Mostaghel N, Davis T (1997) Representations of Coulomb friction for dynamic analysis. *Earthq Eng Struct Dyn* 26:541–548
 38. Ismail M, Casas JR (2016) Evaluation and refinement of closely spaced buildings' performance under near-fault ground motions. *Struct Infrastruct Eng* 12:21–44
 39. China Standard, GB 20688.3-2006 (2006) Rubber bearing-Part 3: Elastomeric seismic-protection isolators of buildings., Beijing
 40. Standard China (2006) JT/T 663-2006. Series of elastomeric pad bearings for highway bridges, Beijing
 41. Standard China (2010) GB 50011-2010. Code for seismic design of buildings, Beijing